17th World Conference on Nondestructive Testing, 25-28 Oct 2008, Shanghai, China

Image processing techniques for ultrasonic inspection

Hartmut KIECKHOEFER, Jan BAAN, Arjan MAST, Arno W.F. VOLKER

TNO Industry & Technology, PO Box 155, 2600 AD Delft, The Netherlands
E-mail: hartmut.kieckhofer@tno.nl, jan.baan@tno.nl, arjan.mast@tno.nl, arno.volker@tno.nl

Abstract

Manual inspection of ultrasonic evaluation images can not only be a time-consuming and therefore expensive task, it can also suffer from operator performance. In this work we apply image processing techniques to automatically inspect ultrasonic C-scan images. Our method is based on the comparison of a C-scan image with a reconstructed reference image. The method was tested on a set of C-scan images with known defects and was able to detect all defects. The number of false detections is still high and will be addressed in future research.

Keywords: image processing, ultrasonic inspection, C-scan images, automated interpretation, ROC parameters

1. Introduction

The turnaround time for ultrasonic inspections is often increased by the time needed for interpretation. Ultrasonic images that need to be interpreted originate from for instance ultrasonic intelligent pipe inspection gauges and ultrasonic C-scan equipment. Interpretation is often done in a non-automated way by a human interpreter carefully analyzing plotted data. This has its drawbacks in terms of speed, accuracy and objectiveness [1]. Image processing techniques for the automatic detection, interpretation and quantification have a number of advantages. Besides the increased speed of interpretation, they give immediate feedback on the production quality which helps to maintain constant production and thus reduce cost.

The idea of using image processing techniques in ultrasonic inspection is not new. Past efforts can broadly be grouped into either improving the visualisation of NDE images to aid visual inspection, e.g. [2–6], or to realise the more challenging task of automated inspection [6–8].

Depending on the specific problem at hand, researchers have developed and utilised various image processing techniques. For data containing low noise levels, Cornwell and McNab [7]

used simple thresholding to segment defects. Corneloup et al [2] worked with textured images and utilised a statistical method assessing spatial amplitude correlation to separate defects from the texture. Swamy and Balasubramaniam [5], on the other hand, processed the Fourier transform of C-scan images with a directional filter bank to separate directional components from the image. Legendre et al [3] applied a wavelet transform to A-scans to reduce structural noise in C-scans of reinforced composites. Pfleiderer et al [4] used a correlation-based method to identify shape and location of a delamination defect in glass-fibre reinforced aluminium (GLARE®), followed by simple matrix manipulation to remove background noise and enhance contrast. Hasanzadeh et al [6], studying human visual perception, derived a fuzzy clustering method to reduce noise and segment defects in NDE images. Dogandžić and Zhang [8] used a Markov chain Monte Carlo algorithm within a Bayesian frame work to estimate shape, location and reflectivity parameters of defects.

Our approach to ultrasonic inspection is derived from the understanding that defects are a deviation from local regular structure visible in an NDE image. A reference image containing this regular structure, reconstructed from the actual measurements, represents therefore a valuable starting point for automatic defect detection. This concept has already proved successful [9], and we will report our development approach, implementation work, test results and conclusions in the following sections.

2. Development approach

The performance of an automated interpretation system, e.g. its capability to *detect* a defect of some type, can be quantified by the *true positive rate* (TPR) or *detection rate*, and the *false positive rate* (FPR) or *false alarm rate*. For more information on these *receiver operating characteristics* (ROC) see Fawcett, [10]. The detection rate is the fraction of defects found during manual inspection that were also detected during automated interpretation. The false alarm rate is the fraction of automatically detected defects that are in fact false detections rather than genuine defects. A perfect classification system would achieve a detection rate of 1 and produce 0 false alarms. However, in practice this can usually not be achieved, see e.g. [9, 11–14] but one has to make a compromise between detection rate and false alarm rate.

Figure 1 shows an ROC curve typical for real-world classification system: Both detection rate and false alarm rate are a function of the system parameters and intrinsically linked. The choice of the system parameters determine the position on the ROC curve.

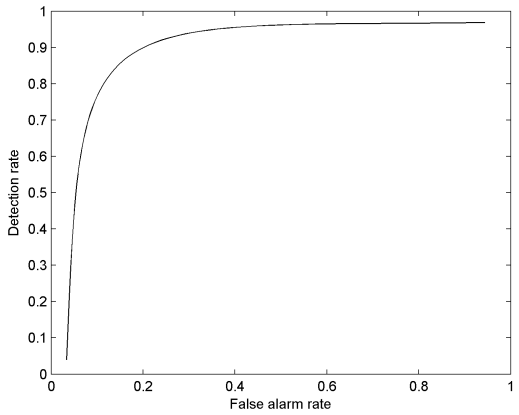

Figure 1. Typical performance of a classification systems visualised in an ROC curve. False alarm rate and detection rate vary as function of the system parameters.

In order to establish the system performance one has to estimate TPR and FPR. To that end, a *ground truth* is required, indicating defect location and type. This ground truth will have to be established manually by an expert. During the system performance evaluation one should also bear in mind the influence of the human factor on manual inspection results [1]: Discrepancies between automatic and manual inspection may require double checking the ground truth.

3. Implementation

We understand defects visible in ultrasonic C-scan images as deviation from local regular structure. To automatically detect these defects we try to construct a reference image containing only regular structure. The deviations between reference image and C-scan image represent potential defects which should include all genuine defects, but will also include artefacts, i.e. false detections. The potential defects are then filtered so that finally, and ideally, only genuine defects are reported. Our approach is summarised in Figure 2.

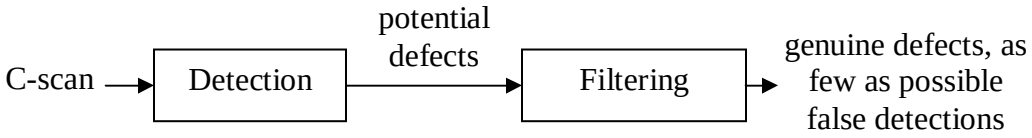

Figure 2. Approach to automated inspection.

3.1 Detection of potential defects

Figure 3 shows a section of a GLARE® C-scan image typical for the data we have been working with. The image features horizontal and vertical structures as well as homogeneous

regions. To realise the first processing step, the detection of deviations from the regular image structure, we build a reference image by modelling the image structure with a morphological directional filter bank.

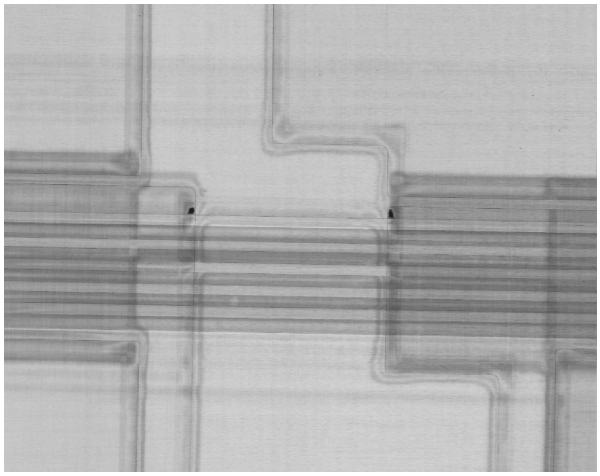

Figure 3. Example of GLARE® C-scan image.

The filter bank consists of three different size morphological closing filters, [15], that decompose the image into horizontal structure, vertical structure and direction-independent structure, see also Figure 4. The reference image is obtained by taking the minimum of the three closing filters at each pixel location. Figure 5 shows the reference image that is estimated with this filter bank from the C-scan image shown in Figure 3.

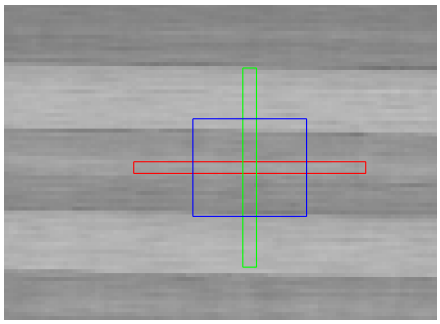

Figure 4. Shapes of the three morphological closing filters.

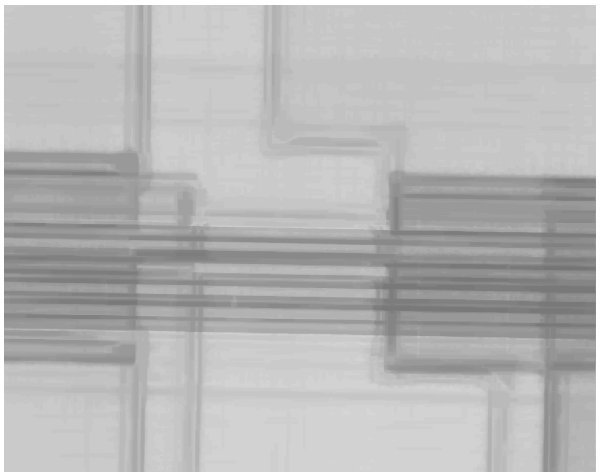

Figure 5. Reference image of the C-scan image in Figure 3, estimated by the morphological filter bank.

To obtain the deviations from the regular structure in the C-scan image one can now take the difference between the reference image and the original C-scan image. The image obtained is the so-called difference image, shown in Figure 6. In our application, the expert, when suspecting a defect, estimates the mean attenuation of a healthy reference area close by and compares it with the maximum attenuation in the suspected defect area. If the difference exceeds a detection threshold the defect hypothesis is confirmed and a second, lower threshold is applied to determine the size of the defect. We applied the same method to the difference image: Using morphological reconstruction we can use the same two thresholds to segment the difference image into potential defects and healthy area. The result of the morphological reconstruction of the difference image from Figure 6 is shown in Figure 7.

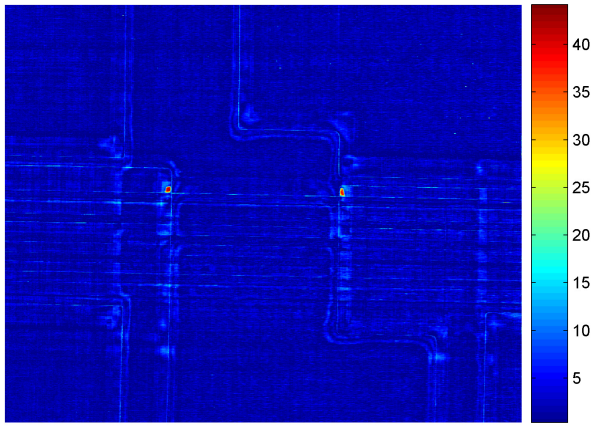

Figure 6. Difference image obtained by subtraction of C-scan image from the reference image. It shows the deviations from the regular structure in the C-scan image, measured in dB.

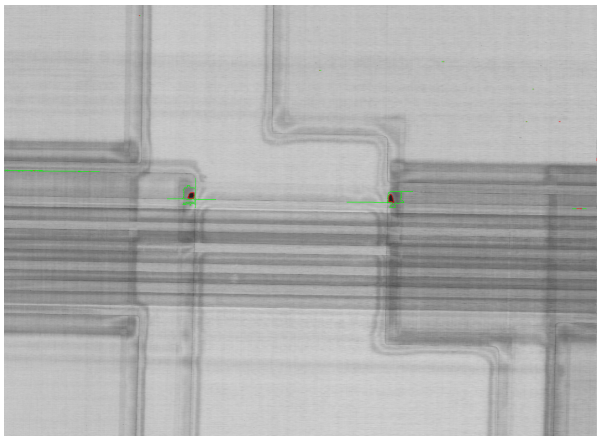

Figure 7. Potential defects detected in C-scan image. Red contours indicate areas where the attenuation in the difference image exceeds the detection threshold, green contours indicate the size of the potential defect based on the sizing threshold.

3.2 Filtering of potential defects

If we compare the detected potential defects (Figure 7) with the defects found during manual inspection (Figure 8, top row), we find that the potential defects include the two genuine defects but also a number of false detections. The aim of the filtering step is now to classify potential defects into genuine defects and false detections so that at the end of the automated inspection only genuine defects are reported.

Filtering of potential defects is based on their image features. These features can be derived from the manual inspection procedure. We use size and aspect ratio of the detections, both properties that can easily be measured with image processing techniques. At the end of the filtering step all false detections were removed for the example shown in Figure 7 and only the genuine defects are reported (see Figure 8, middle row), though their size (green contour) is overestimated.

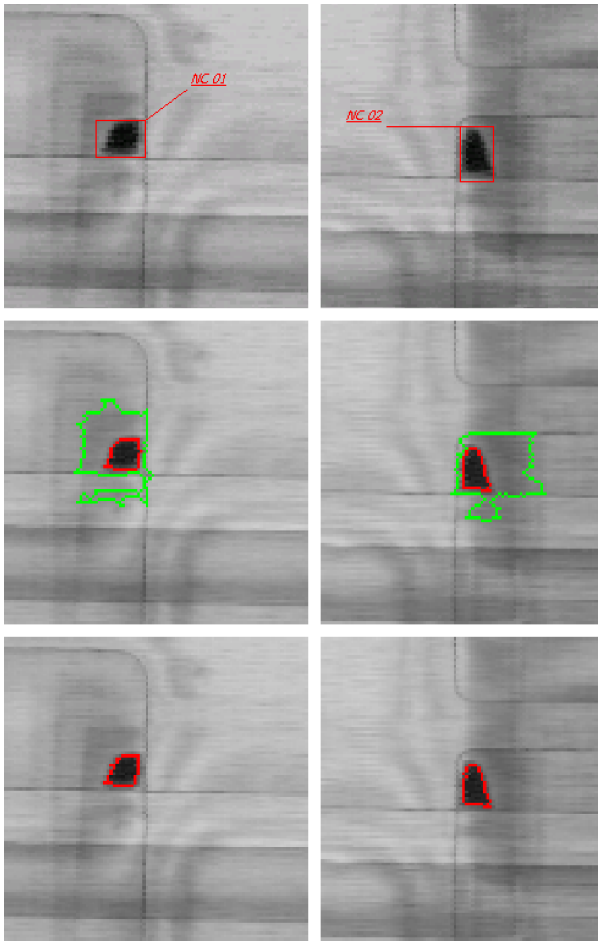

Figure 8. Top row – defect ground truth of image in Figure 3, middle row – automatically detected defects after filtering step (red contours enclose areas where the attenuation exceeds the detection threshold, green contours enclose areas where the attenuation exceeds the sizing threshold), bottom row – defect contour after re-classifying the original defect area (area within the green contour).

4. Results

Our method for automated inspection was implemented as described in section 3 and applied to 21 different GLARE® C-scan images that contained a total of 41 genuine defects. Table 1 summarises the results of the automated inspection. Our approach of detection and filtering was able to detect all genuine defects. However, the number of false detections, although already reduced by the filtering step, is still very large.

It was found that many of the false detections are located in the area of narrow structural lines, structure intersections and in the edge area of the work piece. Other false detections were caused by intended structural deviations such as pilot holes, which were detected and reported as defects.

Table 1. Results of automated C-scan inspection on test set with 41 defects

	automatically detected defects		
	total	missed defects	false detections
after detection	390	0	349
after filtering	252	0	211

5. Options for further improvements

To solve the problem of false detections one could use the structural information available in the work piece overlay file as a priori knowledge to guide the reference image construction and weight the detection features in the filtering step depending on their locality. Furthermore, the number of detection features used in the filtering step could be expanded to include the distance to other detections, attenuation level and gradient properties along the detection contour.

It was also observed that the automatic inspection could overestimate the size of defects if these were in the area of structural features (see Figure 8, top and middle row). This was caused by local imperfections in the constructed reference image. The aforementioned proposals might well be able to solve this problem. Another strategy could be to separate the attenuation readings of the automatically detected defect area into classes based on the spread of their distribution and their spatial distribution. If the result are closed regions we can update the defect contour (see Figure 8, bottom) and obtain defect detections that are even more accurate than the manual defect annotations of the expert.

6. Conclusions

In this paper we presented an approach for automated analysis of ultrasonic C-scan images. The approach is based on image processing techniques which estimate a reference image and then analyse the differences between C-scan and reference image. The approach was tested on a limited set of C-scan images of glass-fibre reinforced aluminium. All genuine defects were detected; however, the number of false detections is still considerable and must be reduced to achieve a genuine reduction in inspection time and hence cost. To that end, a number of proposals were made that will be investigated in future research. Another aspect of our future research will deal with defects that are not sufficiently characterised by attenuation differences and therefore require a different image processing approach.

Acknowledgements

The authors would like to thank Dr. Maarten Bakker (Delft University of Technology, The Netherlands) for organising funding for this research and Stork N.V., The Netherlands, who made C-scan data available and offered expert opinion on C-scan image evaluation.

References

[1] R.A. Murgatroyd, G.M. Worrall, S. Crutzen, Lessons learned from the PISC III study of the influence of human factors on inspection reliability, 6th European Conference on Non-Destructive Testing, 1994, Proceedings, p989-993

[2] G. Corneloup, J. Moysan, I.E. Magnin, Bscan image segmentation by thresholding using cooccurence matrix analysis, Pattern Recognition 29, 1996, p281-296

[3] S. Legendre, J. Goyette, D. Massicott, Ultrasonic NDE of composite material structures using wavelet coefficients, NDT&E International 34, 2001, p31-37

[4] K. Pfleiderer, J. Aufrecht, I. Solodov, G. Busse, Multi-frequency ultrasonic NDE for early defect recognition and imaging, IEEE Ultrasonics Symposium, 2004, p693-696

[5] G. Swamy, K. Balasubramaniam, Directional filter bank-based segmentation for improved evaluation of non-destructive evaluation images, NDT&E International 40, 2007, p250-257

[6] R.P.R. Hasanzadeh, S.H.H. Sadeghi, M.H. Moradi, M. Ahmadi, A density-based fuzzy clustering technique for non-destructive detection of defects in materials, NDT&E 40, 2007, p337-346

[7] I. Cornwell, A. McNab, Towards automated interpretation of ultrasonic NDT data, NDT&E International 32, 1999, p101-107

[8] A. Dogandžić, B. Zhang, Bayesian NDE Defect Signal Analysis, IEEE Transactions on Signal Processing 55, 2007, p372-378

[9] D. Mery, O. Medina, Automated Visual Inspection of Glass Bottles Using Adapted Median Filtering, International conference on Image Analysis and Recognition 2004, Proceedings, Part II, Springer Lecture Notes in Computer Science, Volume 3212, Springer 2004, p818-825

[10] T. Fawcett, An introduction to ROC analysis, Pattern Recognition Letters 27, 2006, p861-874

[11] H.-D. Lin, Automated defect inspection of light-emitting diode chips using neural network and statistical approaches, Expert Systems with Applications (2007), doi:10.1016/j.eswa.2007.09.014

[12] T.W. Liao, Y. Li, An automated radiographic NDT system for weld inspection: Part II—Flaw detection, NDT&E International 31, 1998, 183-192

[13] T. Kubota, P. Talekar, T.S. Sudarshan, M. Xianyun, M. Parker, M. Yuefei, An automated defect detection system for silicon carbide wafers, SoutheastCon, 2002, Proceedings IEEE, p42-47

[14] P.J. Phillips, W.T. Scruggs, A.J. O'Toole, P.J. Flynn, K.W. Bowyer, C.L. Schott, M. Sharpe, FRVT 2006 and ICE 2006 Large-Scale Results, National Institute of Standards and Technology, NISTIR 7408, 2007

[15] J.C. Russ, The image processing handbook, 5th edition, CRC Press, 2007